Structure of Cage Amines as Models for Twisted Intramolecular Charge-Transfer States

Gottfried Köhler,* Karl Rechthaler, and Gottfried Grabner

Institut für Theoretische Chemie und Strahlenchemie, Universität Wien, Althanstrasse 14, A-1090 Vienna, Austria

Roman Luboradzki, Kinga Suwińska, and Krystyna Rotkiewicz

Institut of Physical Chemistry, Polish Academy of Sciences, Kasprzaka 44, PL-01−224 Warsaw, Poland

Received: February 7, 1997; In Final Form: June 25, 1997[⊗]

6-Cyanobenzquinuclidine (CBQ) is widely assumed to be a good model to study twisted internal charge transfer (TICT), a hypothesis proposed to explain the appearance of solvent-induced dual fluorescence in 4-(*N,N*-dimethylamino)benzonitrile (DMABN) derivatives. This is due to the orthogonal arrangement of the nitrogen lone pair and the aromatic π orbitals in this cage amine and the exclusive appearance of long wavelength TICT fluorescence. Spectral and photophysical properties of CBQ are investigated by stationary and time-resolved fluorescence spectroscopy as a function of solvent polarity. The results are discussed in the context of conformational analysis studies performed for CBQ and benzquinuclidine by X-ray crystallography as well as by semiempirical calculations. It is shown that only one singlet excited state is emissive. Fluorescence spectra and intersystem crossing rates can be modeled as charge recombination processes, and excellent agreement between simulated and measured data is found. Rehybridization of the amino group, which leads to a less pyramidal geometry, and torsional vibration about the bond linking the donor group and the benzonitrile moiety contribute essentially to intramolecular charge separation and recombination processes.

1. Introduction

4-(*N,N*-Dimethylamino)benzonitrile (DMABN) shows dual fluorescence in polar solvents.[1] Besides emission from the primary excited state, a second long wavelength fluorescence is observed, which is attributed to a relaxed twisted charge-transfer (TICT) state.[2] The TICT state of DMABN, a molecule that is planar in its ground state, is characterized electronically by almost full charge separation between the electron-donor (dimethylamino) and the electron-acceptor (cyanophenyl) group and geometrically by an orthogonal arrangement of both subunits.

The nitrogen lone pair of the rigid amino group in 6-cyanobenzquinuclidine (CBQ, see Scheme 1) lies within the aromatic plane, and CBQ is thus proposed to be a model compound for the excited rotamer of DMABN. In accordance with the TICT hypothesis, only long wavelength fluorescence is observed for CBQ, appearing in the same energy region as the long wavelength emission of DMABN. This emission was thus attributed to radiative back electron transfer from the TICT state to the electronic ground state.[3]

Direct charge-transfer absorption might be observed for CBQ because of the rigid structure forcing the amino group in a perpendicular conformation relative to the aromatic system. A weak absorption has indeed been found at the long wavelength edge of the aromatic $\pi^* \leftarrow \pi$ transition and was ascribed to the respective promotion of a nitrogen lone pair electron into a π^* orbital located on the aromatic ring.[3]

CBQ fluorescence shows a large Stokes' shift, which amounts to 9000 cm^{-1} in nonpolar solvents. This shift is even larger than that reported for 3,5-dimethyl-(*N,N*-dimethylamino)benzonitrile (3,5-DMDMABN), another pretwisted model compound for a TICT state. A value of 6500 cm^{-1} was found for 3,5-DMDMABN in hexane solution. As in the ground state the amino group of this compound is tilted by ≈70° relative to the aromatic plane, a larger rearrangement energy and thus a larger Stokes' shift was expected for this molecule in comparison to CBQ.[3,4]

SCHEME 1

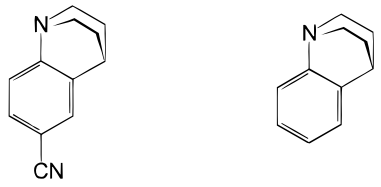

CBQ BQ

In the case in which the amino lone pair lies within the aromatic plane, the transition moment of the respective $\pi^* \leftarrow$ n (TICT) transition should become zero, due to the zero spatial overlap of the terminating orbitals.[5] Rotation of the amino group about the bond connecting the nitrogen atom to the aromatic ring should increase the transition probability due to vibronic coupling to the $\pi^* \leftarrow \pi$ transition but is assumed to be strongly restricted in caged amines.

The knowledge of ground- and excited-state equilibrium geometry of the molecule and of its rigidity appears to be crucial, when the photophysical properties of CBQ are described by the TICT model. It appears essential to characterize distortional motions accounting for a nonzero transition dipole moment and for the large Stokes' shift of CBQ fluorescence. A comparison to benzquinuclidine (BQ) could show the influence of an electron-withdrawing substituent on geometry and vibrational modes, which might be essential in the stabilization of the TICT state. For this purpose, crystallographic analysis of the structure of both compounds was performed, and the results are compared to semiempirical calculations in ground and excited states. Solvent polarity is a further important coordinate for intramolecular charge transfer due to the stabilization of highly dipolar structures. Therefore, the photophysical properties of

[⊗] Abstract published in *Advance ACS Abstracts,* October 1, 1997.

S1089-5639(97)00498-2 CCC: $14.00

CBQ were measured in detail in various solvents and are treated by a detailed model to describe spectral properties and excited-state decay paramteres in relation to various relaxational modes. The results are discussed in comparison to molecular structure information obtained by the two other techniques.

2. Experimental Section

2.1. Materials. 6-cyano-1,4-ethano-2*H*-3,4-dihydroquinoline (CBQ) was synthesized according to ref 6 and additionally purified by recrystallization from hexane. BQ 1,4-ethano-2*H*-3,4-dihydroquinoline (BQ) was purified by sublimation in vacuo.[6] All solvents were of best available quality. They were checked for impurities and purified by standard methods when necessary.

2.2. Fluorescence Measurements. Fluorescence measurements were performed as described previously.[7,8] Time-correlated single-photon counting was used to obtain fluorescence decay profiles. The experimental setup and the deconvolution procedure were described elsewhere.[9] Plots of weighted residuals and of the autocorrelation function, reduced χ^2-values, and mean errors were used to judge the quality of the fit.[10]

2.3. X-ray Crystal Structures. *BQ*. $C_{11}H_{13}N$, monoclinic $P2/_1c$, $a = 782.4(3)$ pm, $b = 1797.0(6)$ pm, $c = 618.6(3)$ pm, $\beta = 108.28°$, $V = 0.826$ nm^3, $Z = 4$, $T = 223$ K, graphite monochromated Mo Kα radiation, λ(Mo Kα) = 71.073 pm, $\rho_x = 1280$ kg m^{-3}, $F(000) = 344$, μ(Mo Kα) = 0.697 cm^{-1}. A single colorless crystal of dimensions $0.1 \times 0.2 \times 0.5$ mm was used for X-ray data collection on an automatic Enraf-Nonius CAD4 diffractometer. 1616 reflections were collected, 1432 of which were unique. The structure was solved by direct methods (MULTHAN11/82[11]) and refined by full-matrix least squares with the SDP system.[12] In final stages of refinement, the non-hydrogen atoms had anisotropic thermal parameters. The hydrogen atoms were "riding" on their carbons at a fixed distance of 108 pm and isotropic temperature factors $U = 0.03$. The final *R*-factor was 0.063, $w_R = 0.062$ ($w = 1/\sigma^2(F_o)$), for 1018 observed reflections with $I_0 \geq 3\sigma(I_0)$ and 148 parameters. Maximum and minimum $\Delta\rho$ on the final difference map were 0.28 $e_0 \cdot Å^{-3}$ (280 $e_0 \cdot nm^{-3}$) and -0.30 $e_0 \cdot Å^{-3}$ (-300 $e_0 \cdot nm^{-3}$), respectively (max. shift/error 0.05).

CBQ. $C_{12}H_{12}N_2$, triclinic P1, $a = 657.5(2)$ pm, $b = 795.6(3)$ pm, $c = 987.5(3)$ pm, $\alpha = 90.42(3)°$, $\beta = 107.21(3)°$, $\gamma = 101.99(3)°$, $V = 0.480$ nm^3, $Z = 2$, $T = 223$ K, graphite monochromated Cu Kα radiation, λ(Cu Kα) = 154.178 pm, $\rho_x = 1270$ kg m^{-3}, $F(000) = 196$, μ(Cu Kα) = 5.61 cm^{-1}. A single colorless crystal of dimensions $0.3 \times 0.3 \times 0.4$ mm was used for X-ray data collection on an automatic Enraf-Nonius CAD4 diffractometer. 2132 reflections were collected, 1896 of which were unique. The structure was solved by direct methods (SHELXS86[13]) and refined by full-matrix least squares with SHELX76.[14] In final stages of refinement the non-hydrogen atoms had anisotropic thermal parameters. The hydrogen atoms were refined with isotropic temperature factors. The final *R*-factor was 0.058, $w_R = 0.065$ ($w = 1/\sigma^2(F_o) + 0.0001F_0$), for 1739 observed reflections with $F_0 \geq 4\sigma(F_0)$ and 175 parameters. Maximum and minimum $\Delta\rho$ on the final difference map were 0.21 $e_0 \cdot Å^{-3}$ (210 $e_0 \cdot nm^{-3}$) and -0.26 $e_0 \cdot Å^{-3}$ (-260 $e_0 \cdot nm^{-3}$), respectively (max. shift/error 0.02).

2.4. Semiempirical Calculations. Semiempirical calculations were performed using the AM1 method in the MOPAC 6.0 implementation including configuration interaction for excited-state calculations.[15−17] Ground-state geometries were fully optimized within the AM1 scheme on the SCF level.

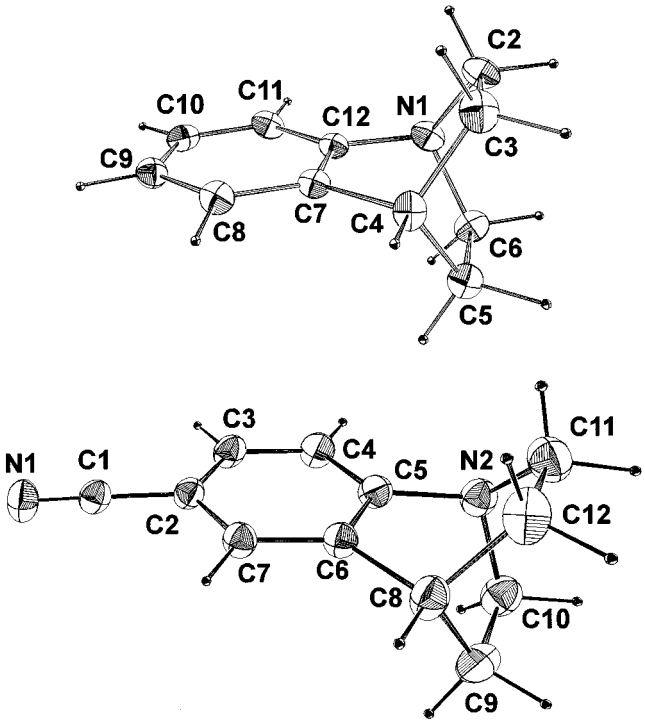

Figure 1. ORTEP perspective drawing of the crystallographic structures of BQ (a, top) and CBQ (b, bottom).

Excited states were calculated including all 100 configurations constructed from the three highest occupied and the two lowest unoccupied orbitals. Parameter sets were the same for ground- and excited-state calculations. Excited-state geometries were optimized for the lowest (π,π^*)-state and the second excited singlet corresponding to the intramolecular charge-transfer state in which an electron is promoted from the nitrogen lone pair into the lowest unoccupied π orbital.

3. Results and Discussion

3.1. Molecular Structures. The molecular structures of BQ and CBQ were obtained by X-ray crystallography, and the results are shown in parts a and b of Figure 1, respectively.

The elementary cells of CBQ and BQ belong to different groups of symmetry, and crystal packing is considerably different for both compounds. No specific intermolecular interactions between the molecules, as, for example, dimer formation, can be deduced from these plots.

Bond lengths and bond angles resulting from the X-ray data are compared to those obtained from semiempirical AM1 calculations. The data agree excellently for both molecules, and deviations are generally smaller than 2% with one exception: the length of the aromatic bond that belongs to both the aromatic and the quinuclidine moiety (C5−C6 for CBQ and C7−C12 for BQ) results slightly larger from semiempirical calculations than in the crystal. The phenyl ring does not differ significantly from hexagonal geometry (bond lengths 139.5 pm and angles 120°), but small length variations within the aromatic ring are observed (for CBQ the longest bonds are C5−C6 pm and C2−C7, the shortest C4−C5 and C6−C7). Because of this good agreement between crystallography results and semiempirical calculations, the molecular geometry in the gas phase and in the crystal can be assumed to be essentially similar.

The geometry of the quinuclidine moiety is distorted non-regularly in both amines. Bond lengths and angles have similar values, and also the pyramidalization angle is nearly identical in both cases. In the ground state the amino group is, thus,

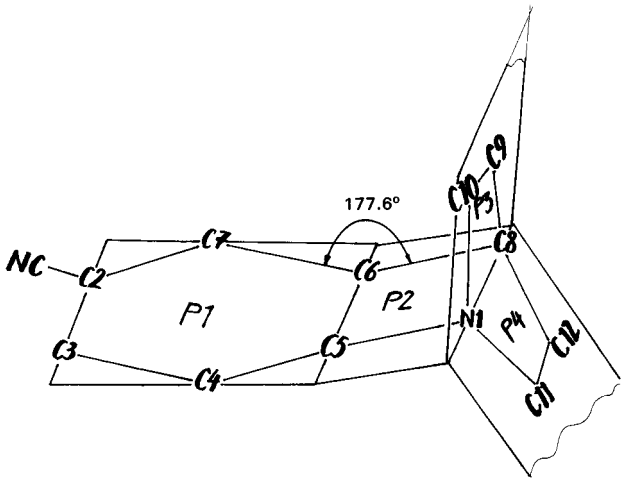

Figure 2. Schematic representation of the P1 and P2 planes in CBQ and of the nonplanarity of the molecule in the crystal.

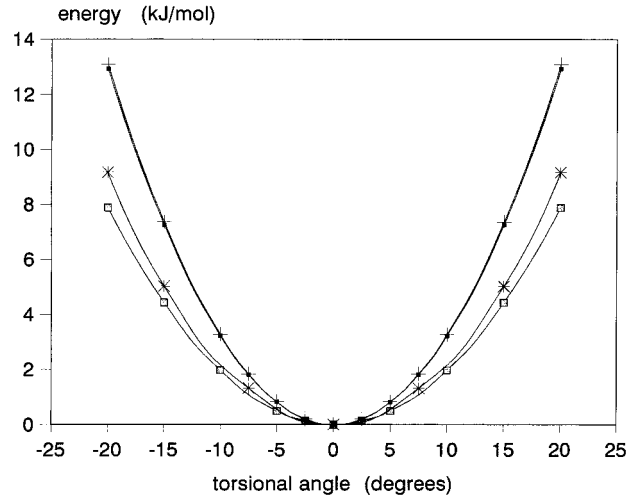

Figure 3. Dependence of the potential energy of CBQ on the dihedral angle (C10, C11, C12, N1) for the ground state of BQ (+), the ground state of CBQ (■), the S_1 state of CBQ (□), and the S_1 of BQ (*).

essentially pyramidal, and this is due to the strong steric strains within the cage. Internal strain causes also a marked deviation of the angles between the bonds connecting the nitrogen or the carbon atom to the ring and aromatic bond; the angles N2−C5−C6 and C8−C6−C5 in the case of CBQ deviate markedly from 120° (i.e. by −4.6° and −7.8°, respectively), whereas the angles N2−C10−C9 and N2−C11−C12 for CBQ, N1−C6−C4 and N1−C2−C3 for BQ are larger than expected for tetrahedral symmetry. Deformations of the other angles within the quinuclidine cage, i.e., C8−C12−C11 and C8−C9−C10 for CBQ, C4−C3−C2 and C4−C5−C6 for BQ, are negligible.

Another important structural deformation might be of greater relevance in the discussion of the TICT excited state in CBQ: the normals to the root-mean-square planes formed by either the six aromatic carbon atoms (P1) or the atoms C5, C6, N2, and C8 (P2) accept an angle of 2.4(1)° (see Figure 2). Such a deformation might induce nonzero orbital overlap between the nitrogen lone pair and the aromatic orbitals. The deviation from coplanarity of P1 and P2 is larger for CBQ than for BQ (for BQ the corresponding angle is just 1.27(2)°).

Geometry minimization within the AM1 scheme does not give any deviation from C_s symmetry, i.e., coplanarity of P1 and P2, and it might thus be proposed that this effect results from crystal packing, which is different for both molecules. The noncoplanarity of the P1 and P2 planes results, however, in a breaking of symmetry for both molecules, and they become consequently chiral. Two enantiomeric forms occur in the crystal because of the appearance of a center of symmetry within the elementary cell. Neither the difference maps nor the observed thermal parameters suggest dynamic or static disorder corresponding to the interconversion of both enantiomeric forms.

3.2. Semiempirical Calculations. Contrary to crystallography, the AM1 calculations yield C_s symmetry for CBQ as well as BQ with a plane of symmetry identical with the aromatic plane. No double well potential is obtained altering the C10−C11−C12−N1 dihedral around 180°. The respective potential energy in dependence of this dihedral angle is shown in Figure 3.

The differences between CBQ and BQ are insignificant, and the energy increase due to this distortion is only small. It amounts to less than 8 kJ mol^{-1} for distortions up to 15°. The dipole moment of CBQ, $\mu = 12.1 \times 10^{-30}$ C m increases by less than 1% and a distortion of 15°. The carbon atom C8 does not change essentially its position during this motion but the amino lone pair twists out of the aromatic plane. Such a motion appears to be feasible both in the ground- and excited-state and induces coupling between the amino lone pair and the aromatic π-orbitals.

Vertical excitations were calculated for the optimum ground-state geometry using an extended configuration interaction scheme between all 100 microstates that can be constructed from the three highest filled orbitals, corresponding to the nitrogen lone pair and two π orbitals, and the two lowest unoccupied aromatic orbitals. The heat of formations obtained for the optimum ground state becomes 227.77 kJ mol^{-1}, and the vertical excitation energy to the lowest singlet state is found at 287.4 nm, in excellent agreement with optical absorption. This transition is of π,π^*-character. It was shown previously that the respective n,π^* state is obtained at higher energies as long as the amino group remains pyramidal.[18] It is observed as the third excited state at 241.6 nm. Only in the case in which the amino group is kept planar in DMABN and perpendicular to the aromatic ring, the $^1A_2$(n,π^*) state, corresponding to the TICT state, becomes the lowest state. It should be pointed out that the calculated vertical transition energies correspond to the maximum of the Franck−Condon envelope of the bands in the gas phase.

The S_1 $^1(\pi,\pi^*)$ excited state of CBQ was minimized within this CI scheme and its optimum energy becomes 638.15 kJ mol^{-1} (the transition energy corresponds to 294 nm), and this yields relaxation energies between the Franck−Condon state and the respective thermalized excited or ground state smaller than 4 kJ mol^{-1} (i.e., 330 cm^{-1}) . The geometries do not change significantly upon optimization. Torsional motions about the C4−C5 bond becomes, however, slightly more feasible in the excited state, as seen from Figure 3.

Optimization of the excited charge transfer state, i.e., the third excited singlet state ^{1}(n,π^*), changes the molecular geometry significantly and reduces its energy to 675.7 kJ mol^{-1}. In the vertical spectrum this state is nearly degenerate with the π,π^*-singlet (290 and 291 nm, respectively), and the charge-transfer state becomes most likely the lowest state in solution because of solvent stabilization due to its large dipole moment, which results as $\mu = 61 \times 10^{-30}$ C m for the vertical Franck−Condon state and decreases due to skeletal relaxation to become $\mu = 56 \times 10^{-30}$ C m in the thermal equilibrium. In this state the amino moiety becomes considerably less pyramidal than in the ground state, and this causes a strong distortion of the cage: the angle C10−N2−C11 increases and the angle C6−C5−N2 decreases, and they result as 113.5° and 110°, respectively. This

destabilizes the vertical ground state significantly, and the corresponding relaxation energy becomes 47.5 kJ mol^{-1} (4600 cm^{-1}), resulting in a large Stokes' shift of the fluorescence transition. Such a large Stokes'shift was also observed for the fluorescence from the ^{1}(n,3s) Rydberg of quinuclidine (1-azabicyclo[2.2.2]octane, ABCO) in the gas phase,[19] and planarization can be compared to a similar geometrical reorganization reported for the lowest excited state of aliphatic amines. In that case, one lone pair electron is promoted into a Rydberg orbital and the amines become essentially planar upon excitation.[9] Such an excited-state reorganization is thus proposed to account predominantly for the large Stokes' shift of CBQ fluorescence.

The main discrepancy between the results from crystallography and semiempirical methods is the high molecular symmetry obtained for the calculated optimum CBQ and BQ geometries. A nonsymmetric structure could experience energetic stabilization from spatial overlap of orbitals located on the quinuclidine moiety, e.g., the nitrogen lone pair, and aromatic π orbitals, and such interactions could probably be underestimated by the semiempirical method. It is, however, more likely that this distortion results from nearest-neighbor interactions within the crystal, as the respective increase in conformational energy can be couterbalanced by intramolecular van der Waals interactions. Symmetry distortions and subsequent mixing of the nitrogen lone pair and the aromatic orbitals appear, therefore, to be feasible in these rather rigid molecules, and this holds essentially for the excited states.

3.3. Photophysical Properties of CBQ. The absorption spectrum of CBQ resembles a superposition of the absorption spectra of the tertiary amino and the cyanophenyl group: the absorption into the lowest Rydberg state of the quinuclidine moiety appears between the two lowest aromatic $\pi^* \leftarrow \pi$ bands. An additional small absorption is observed at the long wavelength edge of the lowest aromatic band for CBQ solutions in hydrocarbons but not in ethanol. It was attributed to the contribution of the $\pi^* \leftarrow$ n transition, promoting a nitrogen lone pair electron into an aromatic π^* orbital, which should shift hypsochromically upon hydrogen bonding in appropriate solvents.[3] This residual transition probability to the TICT state must be induced by vibrational modes distorting the molecular symmetry and mixing these two orbitals, orthogonal in C_s symmetry. According to semiempirical calculations, such molecular motions are feasible (see Figure 3). For BQ no such long wavelength tail is observed in the absorption spectrum, and this indicates that the absence of an electron-withdrawing substituent shifts the $\pi^* \leftarrow$ n transition to higher energies.

CBQ emits a single broad and structureless fluorescence band, and its position depends strongly on the solvent polarity (see Figure 4).[3] The fluorescence quantum yield Q_f is generally low ($\leq$0.008). Systematic investigations of the fluorescence properties of CBQ in numerous solvents are presented in Table 1. Fluorescence emission from BQ is even much weaker and was, therefore, not studied in detail.

A plot of the fluorescence maxima of CBQ versus the solvent polarity function $(D-1)/(D+2)$ is shown in Figure 4. D denotes the dielectric permittivity of the solvent. Irrespective of the polarity function used, such plots are remarkably nonlinear, and the slope increases significantly at higher solvent polarities. The use of a more complex polarity function as e.g.[20]

$$f(D,n) = (D-1)/(D+2) - p\cdot(n^2-1)/(n^2+2) \quad (1)$$

with $p = 1$ or $^1/_2$ reduces only the scatter of the data due to polarization effects (n is the refractive index of the solvent). The essentially nonlinear dependence of the Stokes' shift on solvent polarity should indicate an increase of the excited-state dipole moment with increasing permittivity. This view is supported by the results of electrooptical measurements of excited-state permanent dipole moments of similar charge-transfer states of related compounds such as 2-methyl-4-(*N*,*N*-dimethylamino)benzonitrile (2-MDMABN) or 2,3,5,6-tetramethyl-4-(*N*,*N*-dimethylamino)benzonitrile (2,3,5,6-DMDMABN),[21,22] as they likewise indicate an increase of the excited-state dipole moment with increasing reaction field strength. Its variation can be estimated from the difference in the slopes of linear lines interpolating the data found in a low- or a high-polarity region, respectively. This treatment yields an dipole moment of 39×10^{-30} C m in nonpolar solvents increasing to reach 61×10^{-30} C m in polar solvents.[21] These estimations are in good agreement with the results obtained by electrooptical measurements, which yield a dipole moment of the CT state of DMABN derivatives varying systematically between 33×10^{-30} C m in nonpolar solvents and 50×10^{-30} C m in 1,4-dioxane or benzotrifluoride.[21]

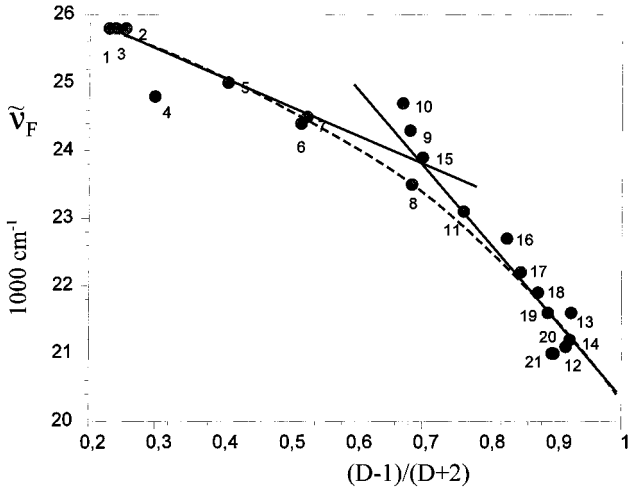

Figure 4. Dependence of the maxima of CBQ fluorescence on the solvent polarity function $(D-1)/(D+2)$. The numbering of solvents is given in Table 1.

TABLE 1: Wavenumber of Fluorescence Maximum ($\tilde{\nu}_f$), Half-Maximum Bandwidth (Γ_f), Fluorescence Lifetime (τ_f), and Transition Dipole Moment of Fluorescence ($\mu_{m\rightarrow n}$) of CBQ in Numerous Solvents

		$\tilde{\nu}_f$, cm^{-1}	Γ_f,[a] cm^{-1}	τ_f, ns	$\mu_{m\rightarrow n}$, 10^{-30} C m
1	hexane	25 800	5900	1.09	2.2
2	cyclohexane	25 800	6200	1.05	2.1
3	isooctane	25 800	6000	1.07	2.2
4	benzene	24 800		1.30	1.9
5	butyl ether	25 000		1.09	2.3
6	*tert*-butyl methyl ether	24 400	5600	0.99	2.5
7	ethyl ether	24 500	6200	1.06	2.5
8	tetrahydrofuran	23 500	4900	1.18	2.4
9	1-chlorobutane	24 300	6200	1.18	2.3
10	1,1,1-trichloroethane	24 700	5800	1.17	2.1
11	dichloromethane	23 100	6000	1.24	1.9
12	1,2-dichloroethane	23 100	6000	1.36	2.2
13	propionitrile	21 000	5300	1.93	2.3
14	acetonitrile	21 600	5500	2.17	2.1
15	*N*,*N*-dimethylformamide	21 200	5300	2.34	1.9
16	1-decanol	23 900	5500	1.47	2.0
17	1-pentanol	22 700		1.79	2.0
18	1-butanol	22 200	5000	1.65	2.2
19	1-propanol	21 900	5600	1.60	2.3
20	ethanol	21 600	5300	1.90	2.2
21	methanol	21 100	5700	2.13	2.3
22	2,2,2-trifluoroethanol	21 000	5500	2.67	2.1

[a] Error limits for Γ_f are $\pm$400 cm^{-1}.

Regarding the uncertainty in determining excited state dipole moments, the experimental values are considered in good agreement with that obtained from semiempirical calculations. The dependence of the dipole moment on the reaction field strength results mainly from a large excited-state polarizability of the molecule. The molecular structure should also depend on the reaction field, as the dipole moment and the polarizability depends on the molecular geometry, and this effect might additionally contribute to the nonlinear dependence of the fluorescence maximum on the solvent polarity function.

Nevertheless, the significant increase in the slope of the solvent polarity dependence of the spectral shift and a strong concomitant increase of the fluorescence lifetime (see Table 1) could also indicate that the character of the excited-state changes with increasing solvent polarity. On the other hand, the fluorescence quantum yield is 0.007 ± 0.001 and nearly independent of solvent properties. The rate constant for the radiative decay follows, therefore, the variation of the reciprocal decay times and is larger in nonpolar than in strongly polar solvents.

The transition dipole moment of fluorescence $\vec{\mu}_{m\rightarrow n}$ can be calculated from eq 2 (Q_f denotes the quantum yield of fluorescence, τ_f its lifetime, and $\tilde{\nu}_f$ its maximum wavenumber; all other constants have their usual meaning)

$$|\vec{\mu}_{m\rightarrow n}| = \sqrt{\frac{3h\epsilon_0}{16\pi^3 n^3 \tilde{\nu}_f^3}\cdot\frac{Q_f}{\tau_f}} \tag{2}$$

and it does not vary systematically with the solvent polarity (see Table 1). Its mean value equals $|\mu_{m\rightarrow n}| = (2.2 \pm 0.3) \times 10^{-30}$ C m. The observed solvent dependence of the radiative decay rate constant results, therefore, mainly from the solvent shift of the fluorescence spectrum maximum, which appears to the third power in eq 2. The transition dipole moment is determined primarily by direct interactions of the charge-transfer state and the ground state and additionally by admixtures from various locally excited states *i*. $\mu_{m\rightarrow n}$ is therefore related to the respective coupling matrix elements, V_{AD} and V_i, and the energy gap between the charge-transfer excited state and the ground state as well as these locally excited states with energy E_i, according to the following formula:[23]

$$\vec{\mu}_{m\rightarrow n} = \frac{V_{AD}(\vec{\mu}_m - \vec{\mu}_n)}{hc\tilde{\nu}_f} + \sum_i \frac{V_i\vec{\mu}_{n\rightarrow i}}{E_i - hc\tilde{\nu}_f} \tag{3}$$

The decrease of the fluorescence peak energy with increasing solvent polarity should cause an increase of the first term, which dominates this expression in most cases, and thus a variation of $\mu_{m\rightarrow n}$ with solvent permittivity results. Nevertheless, V_{AD} is small in the case of a charge-separated excited state, and the magnitude of $\mu_{m\rightarrow n}$ should be significantly influenced by mixing with other states. The second term in expression 3 decreases as fluorescence shifts to lower energies, and this could widely cancel the expected increase of the first term. A systematic variation of the transition dipole moment is, therefore, most likely masked by the error limits, which are large for this complex quantity.

Nevertheless, there is good evidence that fluorescence arises only from one singlet excited state with large charge-transfer character, i.e., a high permanent dipole moment, indicated by the large solvent shift of the spectrum. These findings are in good agreement with the TICT hypothesis.

As CBQ fluorescence can be viewed as thermal intramolecular charge recombination emission, the fluorescence spectrum can be modeled by a formalism, that was first applied to return electron transfer within radical ion pairs and its relationship to the fluorescence spectra of such exciplexes.[24] In this treatment the fluorescence spectrum is given by

$$\frac{I_f}{\nu_f^3} = B\cdot|\vec{\mu}_{m\rightarrow n}|^2\cdot\mathrm{FCF}(\Delta g) \tag{4}$$

and the factor *B* denotes

$$B = n\left(\frac{n^2+2}{3}\right)\cdot\frac{64\pi^4}{3hc^3}\cdot\frac{1}{4\pi\epsilon_0} \tag{5}$$

All constants have their usual meaning. $\mu_{m\rightarrow n}$ is the electronic matrix element for the radiative transition, and FCF denotes the Franck−Condon factor. Its energy dependence resembles the shape of the fluorescence spectrum. In the case of emissive back electron transfer the free energy change is given by:

$$\Delta g = \Delta E_{et} + h\nu_f \tag{6}$$

and ΔE_{et} is the difference between the energy of the optimum excited-state configuration and that of the ground state. It is thus a negative value. The Franck−Condon factors FCF(Δg) can be evaluated explicitly from a model dividing the nuclear motions, affected by the back electron transfer process, into those with frequency lower than k_BT/h, which correspond essentially to reorganization motions of the solvent, and those of higher frequencies associated with skeletal vibrations of the solute.[24] A reorganization energy λ_s is assigned to the low-frequency modes, whereas the high-frequency vibrations are represented by a single averaged mode ν_v and a reorganization energy λ_v.

The thermally weighted sum of FCFs is then given by

$$\mathrm{FCF}(g) = \frac{1}{\sqrt{4\pi\lambda_s k_B T}}\sum_{j=0}^{\infty} F_j \exp\left(-\frac{(\Delta g + jh\nu_v + \lambda_s)^2}{4\lambda_s k_B T}\right) \tag{7}$$

F_j represents the Franck−Condon factor for a single $0 \rightarrow j$ vibronic transition and is given by

$$F_j = \exp(-S)\frac{S^j}{j!} \quad \text{with} \quad S = \frac{\lambda_v}{h\nu_v}$$

The fluorescence spectra of CBQ measured in various solvents are shown in Figure 5 together with a fit of the spectrum in cyclohexane solution as one example for the formalism given above. In this case, the parameters for a best fit to the measured spectrum are $\Delta E_{et} = -32\,000$ cm^{-1}, $\lambda_s = 3200$ cm^{-1}, $h\nu_v = 1600$ cm^{-1}, and $\lambda_v = 3700$ cm^{-1}. The value obtained for $h\nu_v$ corresponds to aromatic C−C stretching vibrations, and these skeletal modes are expected to be most effective in the optical transition. λ_v is in reasonable agreement to the relaxation energy of the ground state after fluorescence found by semiempirical calculations in the gas phase. An energy difference of 4600 cm^{-1} was obtained for the vertical Franck−Condon and the optimum ground state.

The fit parameters for the spectrum obtained in ethanolic solutions are: $\Delta E_{et} = -27\,700$ cm^{-1}, $\lambda_s = 4450$ cm^{-1}, $h\nu_v = 1600$ cm^{-1}, and $\lambda_v = 2150$ cm^{-1}. The decrease in ΔE_{et} corresponds to the stabilization of the excited TICT state due to the larger reaction field of the solvent, and it should also acount for the increase of λ_s. The spectral shift of the fluorescence depends mainly upon ΔE_{et} and λ_s. For the maxima of the fluorescence spectra, 25 700 and 21 650 cm^{-1} were

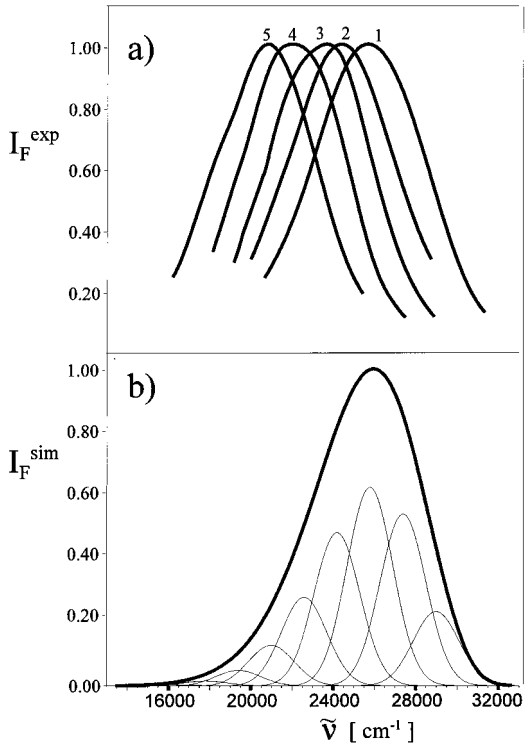

Figure 5. (a) Corrected normalized fluorescence spectra of CBQ in isooctane (1), diethyl ether (2), tetrahydrofuran (3), 1-butanol (4), and 2,2,2-trifluoroethanol (5) and (b) simulated fluorescence spectrum of CBQ in a hydrocarbon solvent according to eq 4 using the following parameters: $\Delta E_{et} = 32\,000$ cm^{-1}, $\lambda_s = 3200$ cm^{-1}, $h\nu_v = 1600$ cm^{-1}, and $\lambda_v = 3700$ cm^{-1}.

recovered from the fit for cyclohexane and ethanol solutions, respectively. This is in excellent agreement with the experimental values (see Table 1).

For CBQ a decrease in the half-bandwidth Γ_f of the fluorescence band with increasing solvent polarity was found (see Table 1), in contrast to the observation that most single fluorescence bands become broader and are smoothed in polar solvents. $\Gamma_f = 6250$ and 5270 cm^{-1} is obtained from this model for the two solvents, respectively, in good agreement with the experimental results compiled in Table 1. A decreasing vibrational reorganization energy λ_v accounts mainly for the decrease in Γ_f, and this should indicate that the energy gap between the minimum ground state and the vertical Franck−Condon state populated after fluorescence decreases, i.e., that geometrical changes due to the relevant skeletal modes are smaller in a polar solvent. In polar solvents the excited-state minimum geometry might be more similar to the ground-state geometry than in a nonpolar environment.

The rate constant for the radiationless decay can also be described within this model of back electron transfer. It was shown earlier for various derivatives of DMABN that intersystem crossing leads to a locally excited state and that the respective rate constant can be explained by the Marcus energy gap rule.[18] Intersystem crossing rates of CBQ were measured by energy transfer to the anthracene triplet in some solvents, i.e., in hexane, acetonitrile,[25] and ethanol. Fluorescence and triplet yields of CBQ have been shown to add up to unity in hexane solution, but $Q_f + Q_T = 0.75$ in ethanolic solution. The intersystem crossing rate constants k_{isc} decrease from $(9.5 \pm 0.5) \times 10^8$ s^{-1} in hexane to $(3.5 \pm 0.2) \times 10^8$ s^{-1} in ethanol.[18] This is in accordance with the decrease of the energy gap between the TICT singlet and the lower $^3\pi,\pi^*$ triplet in the normal Marcus region. As the fluorescence intensity is low and intersystem crossing is efficient, it determines essentially

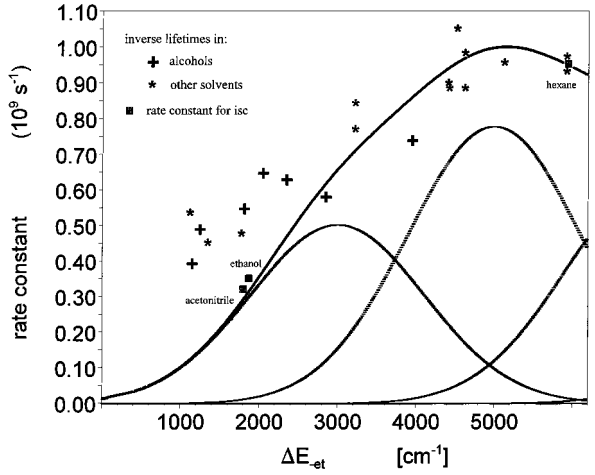

Figure 6. Plot of the inverse fluorescence lifetime $1/\tau_f$, the measured intersystem crossing rate constants in hexane, acetonitrile, and ethanol, and the simulated intersystem crossing rate constants (full line) calculated according to eq 8 versus the energy gap between the TICT state and the lowest triplet (for more details, see text). The dotted lines give the contributions of the accepting skeletal vibrational modes to the rate constant.

the decay of the TICT state and thus its fluorescence lifetime. The measured fluorescence lifetime of CBQ was thus simulated by the following formalism.

The rate constant for a nonradiative decay by back electron transfer is given by

$$k_{-et} = \frac{4\pi^2}{h} \cdot V^2 \cdot \mathrm{FCF}(\Delta g) \qquad (8)$$

and V denotes the electronic matrix element for the nonradiative transition. In the case of intersystem crossing, the free energy change Δg is the electronic energy difference ΔE_{-et} between the TICT state and the terminating triplet, and in the case of internal conversion, that between the TICT and the ground state.

Figure 6 shows the dependence of the inverse fluorescence lifetime in various solvents on the respective singlet − triplet splitting ΔE_{-et}. The intersystem crossing rates measured in the three solvents hexane, acetonitrile, and ethanol are also given in that figure.[18,25] The values of ΔE_{-et} in a hydrocarbon solvent can be estimated from the onset of fluorescence of room-temperature fluorescence and the spectral position of the 0−0 transition of phosphorescence observed in a low-temperature glass. Phosphorescence does not depend on the polarity of glass within the error limits.[18] As the permanent dipole moment in the triplet state is much smaller than in the TICT singlet, this gap should depend predominatly on the shift of fluorescence.

No reasonable set of parameters was found to fit a single nonradiative decay rate, calculated by the formalism described above, to the inverse of the measured fluorescence lifetimes over the whole energy range. The measured intersystem crossing rate constants in ethanol and acetonitile are, however, significantly smaller than the inverse lifetime. Most of the inverse lifetime data and all intersystem crossing rates are, nevertheless, excellently reproduced using the following parameters: ΔE_{-et} (in hexane) $= -5800$ cm^{-1}, $\lambda_s = 3000$ cm^{-1}, $h\nu_v = 2000$ cm^{-1}, and $\lambda_v = 3100$ cm^{-1}.

It is thus concluded that only at high solvent polarities (solvents with larger dielectric permittivity than of a long chain alcohol like hexanol, i.e., $D \approx 14$), an additional radiationless process contributes to the decay of the TICT state, in accordance with the smaller quantum yield of intersystem crossing found in ethanol and acetonitrile solutions. This process is most

probably internal conversion to the ground state, which becomes essential as the energy gap between the TICT and the ground state becomes sufficiently small in high-polarity solvents. This is the Marcus inverted region, and the rate constant of this process increases therefore with a decreasing energy gap. Additional internal conversion to the ground state should thus account for the increasing deviation between simulated intersystem crossing rates and the measured inverse lifetimes in high-polarity solvents. The respective data for ethanolic solutions are $k_f = 7 \times 10^6\ s^{-1}$, $k_{isc} = 3.5 \times 10^8\ s^{-1}$, and $k_{ic} = 1.3 \times 10^8\ s^{-1}$.

The different energies of the effective vibrational modes and the related relaxation energies obtained from the model for radiative and nonradiative back charge-transfer processes show that different reaction ccordinates are involved in both processes. C−C stretching vibrations are the predominant skeletal modes for the radiative decay, whereas higher modes, like, e.g., C−H vibrations, contribute significantly to intersystem crossing ($h\nu_v$ is significantly larger for intersystem crossing in comparison to the fluorescence). The solvent reorganization energy λ_s recovered from the simulation of intersystem crossing lies between the λ_s values found for recombination fluorescence in hexane and ethanol and might, therefore, resemble a mean value for solvents of different polarity.

4. Conclusions

In CBQ the aromatic π-orbitals and the amino lone pair orbital are orthogonal, and it constitutes thus the most fundamental molecule to study twisted intramolecular charge-transfer fluorescence. The TICT phenomenon needs orthogonality of donor and acceptor orbitals, as only in this case is an electron transferred between separated parts of one molecule. In the case in which the terminating orbitals are not orthogonal, they are conjugated and extend over the whole molecule. Nevertheless, to obtain a nonzero electronic matrix element for the radiative transition, it needs at least temporary overlap of the amino lone pair with the aromatic π-orbitals. Although the quinuclidine cage is rather rigid, both the crystal structure and semiempirical calculations show that it is easily deformed at least to a small extent, which causes a small mixing of both orbitals. The observed torsional motion of the amino nitrogen is thus essential for the observation of TICT fluorescence.

The spectrum of this fluorescence can be simulated by a model based on thermal electron transfer theory and separating the basic nuclear motions into two groups, one of the typical frequency for intramolecular vibrations and a second with much smaller energy corresponding to solvent reorganization. Aromatic C−C stretching vibrations are the most important promoting modes for the radiative decay, and the conformational relaxation energy corresponds approximately to two vibrational quanta. This value is in agreement with the respective energy difference between the vertical Franck−Condon state and the ground-state minimum, which is obtained from semiempirical calculations. Rehybridization on the nitrogen, which leads to a less pyramidal geometry in the excited states, accounts for most of this destabilization energy. To reproduce the observed narrowing of the spectra in polar solvents, this energy difference is assumed to become smaller with increasing solvent polarity, and equilibrium geometries in ground and excited states differ, therefore, less in a polar than in a nonpolar solvent. This could be due to the observed decrease in the excited-state dipole moment upon this relaxational mode.

Also the fluorescence lifetimes, which are mainly dominated by back electron transfer intersystem crossing, can be modeled by this approach. In this case, higher vibrational modes, most probably C−N or C−H vibrations, contribute to the coupling of the TICT state to the final $\pi\pi^*$-triplet. At larger solvent polarities, as the energy gap between the TICT excited state and the ground state becomes significantly smaller, good indication for additional internal conversion to the ground state is obtained.

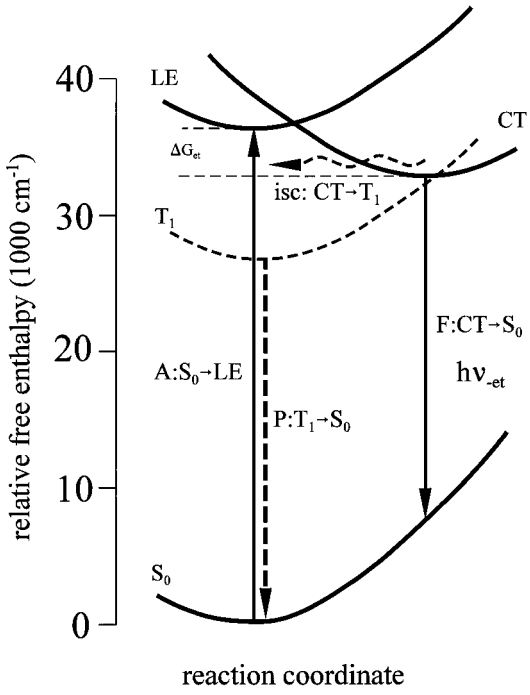

Figure 7. Schematic free energy diagram for CBQ in a hydrocarbon solvent.

The free energy diagram obtained for CBQ in hexane taking the energies from the photophysical model is depicted in Figure 7. A very small barrier separates the vertically excited state and the TICT state, when the same parameters are assumed to control forward electron transfer to popuplate the TICT state as well as back electron transfer to the local triplet state. Formation of the TICT state is, therefore, extremely fast and accounts for the efficient quenching of the local fluorescent state. The maximum of the observed CBQ fluorescence band and that of phosphorescence emission fits also to this diagram. It describes, thus, quantitatively the spectroscopic and photophysical behavior of CBQ.

Acknowledgment. We gratefully acknowledge N. Detzer who supplied us with a sample of CBQ, and A. Krówczyński who supplied a sample of BQ. K.R. and G.K. are indebted to the *Fonds zur Förderung der wissenschaftlichen Forschung in Österreich* for financial support (Proj. Nr. P11880-CHE).

Supporting Information Available: List of structure factors, anisotropic thermal parameters, and hydrogen positional parameters have been deposited with the British Library Document Supply Centre as Supplementary Publication No. SUP 000000. Copies may be obtained through The Technical Editor, International Union of Crystallography, 5 Abbey Square, Chester CH1 2HU, England.

References and Notes

(1) Lippert, E.; Lüder, W.; Boos, H. *Advances in Molecular Spectroscopy*; Mangini, Ed.; Pergamon Press: Oxford, 1962; p 443.
(2) Grabowski, Z. R.; Rotkiewicz, K.; Siemiarczuk, A.; Cowley, D.; Baumann, W. *J. Nouv. Chim.* **1979**, *3/7*, 443.
(3) Rotkiewicz, K.; Rubaszewska, W. *Chem. Phys. Lett.* **1980**, *70*, 444.
(4) Rotkiewicz, K.; Rubaszewska, W. *J. Lumin.* **1982**, *27*, 221.

(5) Lipiński, J.; Chojnacki, H.; Grabowski, Z. R.; Rotkiewicz, K. *Chem. Phys. Lett.* **1980**, *70*, 449. Grabowski, Z. R.; Rotkiewicz, K.; Siemiarczuk, A. *J. Lumin.* **1979**, *18/19*, 420.

(6) Krówczyński, A. *Pol. J. Chem.* **1984**, *58*, 933.

(7) Köhler, G.; Kittel, G.; Getoff, N. *J. Photochem.* **1982**, *18*, 19.

(8) Köhler, G.; Rotkiewicz, K. *Spectrochim. Acta* **1986**, *42A*, 1127.

(9) Köhler, G. *J. Photochem.* **1986**, *35*, 189.

(10) O'Connor, D. V.; Phillips, D. *Time Correlated Single Photon Counting*, Academic Press: New York, 1984.

(11) Main, P.; Fiske, S. J.; Hull, S. E.; Lessinger, L.; German, G.; Declerq, J.-P.; Woolfson, M. M. *MULTAN11/82. A System of Computer Programs for the Automatic Solution of Crystal Structures from X-ray Diffraction Data*; University of York, England, and Louvain, Belgium, 1982.

(12) Frenz, B. A., & Associates, Inc. *SDP. Structure Determination Package*; College Station, TX, and Enraf-Nonius, Delft, The Netherlands, 1985.

(13) Sheldrick, G. M. *SHELXS86. Program for Crystal Structure Solution*; University of Göttingen, Germany, 1986.

(14) Sheldrick, G. M. *SHELX76. Program for Crystal Structure Determination*; University of Cambridge, England, 1976.

(15) Dewar, M. J. S.; Zoebisch, E. G.; Healy, E. F.; Stewart, J. J. P. *J. Am. Chem. Soc.* **1985**, *107*, 3902.

(16) Armstrong, D. R.; Fortune, R.; Perkins, P. G.; Stewart, J. J. P. *J. Chem. Soc., Faraday Trans. 2* **1972**, *68*, 1839.

(17) Dewar, M. J. S.; Stewart, J. J. P *QCPE Bull.* **1986**, *6*, 506.

(18) Köhler, G.; Grabner, G.; Rotkiewicz, K. *Chem. Phys.* **1993**, *173*, 275.

(19) Halpern, A. M. *J. Am. Chem. Soc.* **1974**, *96*, 7655.

(20) Herbich, J.; Waluk, *J. Chem. Phys.* **1994**, *188*, 247.

(21) Baumann, W.; Bischof, H.; Fröhling, J.-C.; Brittinger, C.; Rettig, W.; Rotkiewicz, K. *J. Photochem. Photobiol. A* **1992**, *64*, 49.

(22) Brittinger, C.; Maiti, A. K.; Baumann, W.; Detzer, N. *Z. Naturforsch. A* **1990**, *45*, 1.

(23) Birks, J. B. *Photophysics of Aromatic Molecules*; Wiley-Interscience: London, 1970.

(24) Gould, I. R.; Farid, S.; Young, R. H. *J. Photochem. Photobiol. A* **1992**, *65*, 133 and references cited herein.

(25) Grabner, G. To be published.